Published in final edited form as:
Anal Chem. 2009 November 15; 81(22): 9402–9409. doi:10.1021/ac901820v.

MALDI Mass Spectrometric Imaging using the Stretched Sample Method to Reveal Neuropeptide Distributions in *Aplysia* Nervous Tissue

Tyler A. Zimmerman, **Stanislav S. Rubakhin**, **Elena V. Romanova**, **Kevin R. Tucker**, and **Jonathan V. Sweedler***
Department of Chemistry and the Beckman Institute, University of Illinois, Urbana, Illinois 61801

Abstract

Neuropeptides are a diverse set of complex cell-cell signaling molecules that modulate behavior, learning and memory. Their spatially heterogeneous distributions, large number of post-translational modifications, and wide range of physiologically active concentrations make their characterization challenging. Matrix-assisted laser desorption/ionization (MALDI) mass spectrometric imaging is well-suited to characterizing and mapping neuropeptides in the central nervous system. Because matrix application can cause peptide migration within tissue samples, application parameters for MALDI typically represent a compromise between attaining the highest signal quality and preserving native spatial distributions. The stretched sample approach minimizes this tradeoff by fragmenting the tissue section into thousands of spatially isolated islands, each ~40 microns in size. This inhibits analyte migration between the pieces and, at the same time, reduces analyte-salt adduct formation. Here we present methodological improvements that enable the imaging of stretched tissues and reveal neuropeptide distributions in nervous tissue from *Aplysia californica*. The distributions of known neuropeptides are shown to correspond with previous immunohistochemical results, demonstrating that the stretched imaging method is well-suited for working with easily redistributed molecules and heterogeneous tissues, and reduces adducts from physiological salts.

INTRODUCTION

In contrast to many imaging methods, using mass spectrometry (MS) to image thin tissue sections allows acquisition of both chemical and spatial information without the need to preselect the analyte of interest. Matrix-assisted laser desorption/ionization (MALDI), a soft ionization technique, is suitable for mass spectrometric imaging (MSI) due to its high sensitivity and ease of interpretation; most peptides and proteins are ionized as intact molecular ions. Although tandem MS may be used to discover the sequences of unknown analytes, the high specificity of MS is often sufficient to identify analytes directly by mass matching in specific tissues where the identities of many analytes have already been determined.[1, 2] MALDI-MSI has been used to identify and map analytes in neuronal samples3 containing diverse classes of lipids,4 signaling peptides,[5] hormones,[6] and alternatively spliced forms of proteins.[7] Recently, such studies have revealed the distinct localizations of several neuropeptides in the white and gray matter of rat spinal cord,[8] allowed classification of

* Corresponding author Address: Department of Chemistry, University of Illinois, 600 South Mathews Ave. 63-5, Urbana, IL 61801 Voice: 217-244-7359 Fax: 217-244-8068 sweedler@scs.uiuc.edu .

SUPPORTING INFORMATION AVAILABLE Supporting Information Available: This material is available free of charge via the Internet at http://pubs.acs.org.

tumorous gastric tissue from human patients,[9] and produced two- and three-dimensional molecular ion maps of neuropeptide distributions in the Jonah crab brain.[10]

Compared to their mammalian counterparts, invertebrate models such as *Aplysia californica* have morphologically simpler nervous systems, enabling a more refined focus on the mechanisms of neural plasticity underlying learning, memory, and complex behaviors.[11, 12] In addition, the peptide content of many of the large, reliably identifiable *Aplysia* neurons has been characterized,[2, 13, 14] facilitating validation of the results of MSI experiments. Nonetheless, despite the relative structural simplicity as compared to the mammalian CNS, *Aplysia* CNS tissue samples are biochemically complex and present a number of analytical measurement challenges. For example, the abdominal ganglion has numerous areas where adjacent peptidergic neurons contain unique sets of peptides expressed in varying amounts.[14, 15] Furthermore, the low amounts of some neuropeptides and/or peptides expressed only in a few neurons can be difficult to measure by MS for large tissue areas or for a whole tissue homogenate, especially in the presence of more abundant peptides.[16] Thus, MSI of neuronal samples requires both low detection limits and high spatial resolution.

It is during the matrix application step in traditional MALDI-MSI experiments that meeting these two prerequisites often involves a compromise. Although longer exposure of the sample to MALDI matrix improves peptide signals by allowing better analyte extraction and incorporation into the matrix, it reduces the quality of the resulting MS imaging by allowing analyte redistribution in tissue wetted by the matrix solution.[15, 17] The formation of large matrix crystals over the area containing multiple cells also occurs, preventing more detailed localization than the size of individual matrix crystals. Spatial resolution can be improved by instrumentation advances such as enhanced ion optics.[18] However, limitations resulting from sample preparation and matrix application are not addressed by enhancements to instrumentation. Several approaches that add matrix to tissues using sprayers and droplet generators can address several of these issues,[19-21] but the compromises mentioned above still remain.

With the stretched sample method,[15, 22] we have eliminated the signal and spatial resolution tradeoff issue in imaging experiments. A thin tissue slice is placed on a monolayer of beads embedded in a stretchable membrane. The membrane is then stretched, fragmenting the tissue into thousands of nearly single cell-sized pieces that strongly adhere to each bead. After stretching, the spatial separation of the beads/tissue pieces by the intervening hydrophobic membrane allows longer matrix application periods, thereby preventing analyte redistribution between beads. Providing additional benefit, multiple slow solvent condensation and recrystallization steps reduce relative signal intensities of inorganic ion adducts in the resulting spectra, even in the presence of high physiological salts.[23] Recent findings[24, 25] demonstrate that use of the Parafilm M membrane in MALDI-MS experiments as a surface for analyte deposition and detection can result in increased sensitivity of neuropeptide detection while appropriate membrane treatments significantly increase membrane stretchability.

However, the stretched sample approach can be hampered by nonuniform stretching of the membrane, so that reconstruction of ion images at the original bead positions is not a straightforward process. Thus, prior reports have focused on tissue profiling and the imaging capabilities of this sample preparation approach have yet to be validated. In contrast to standard tissue imaging, the bead locations are not in an ordered array. To achieve tissue imaging, the stretched sample approach has recently been adapted to include computational methods that realign the positions of the molecular ion signals acquired from stretched samples with their locations in the original intact tissue sections.[22] These reconstructed ion images from stretched samples can then be co-registered with the original sample morphology. Also, a recent enhancement in image acquisition speed is accomplished via automated data acquisition—at

the individual bead locations—using sample-tailored geometry files to determine at what locations to acquire spectra. This suite of computational methods[22] has been applied to profile small numbers of peptide-coated beads.

Here we further refine and optimize the stretched imaging method to enable MALDI-MSI of thin tissue sections from the *Aplysia* CNS. Several computational and experimental improvements are made that now allow imaging of stretched biological tissues. We have developed new protocols and applied them to MS imaging of the *Aplysia* ganglia. Importantly, the peptide content of numerous cell populations in the abdominal ganglion has been characterized by traditional molecular biology and immunohistochemical approaches, providing validation of the MS imaging results. Although two other ganglia used in this study, the pleural and pedal, are widely used neurobiological models for studying neural plasticity, [26, 27] they are less well-characterized biochemically, and thus present an opportunity for MALDI-MSI analysis of neuropeptide diversity and localization.

EXPERIMENTAL

Parafilm M Substrate Preparation

Hexagonally closest packed bead monolayer substrates on Parafilm M (Pechiney, Neenah, WI) were prepared containing both blue and clear beads as previously reported.[22] Creating substrates that are appropriate for work with *Aplysia* ganglia sections requires ~10 mg of 40-μm diameter glass beads for an ~1 cm diameter monolayer. An optical image of the entire bead substrate is then taken using a light microscope (Leica Microsystems, Bannockburn, IL). The positions of the beads in the initial (before stretching) sample image are determined via light thresholding as described previously[22] using ImageJ (version 1.38, http://rsb.info.gov/ij) with the Colour Thresholding plugin.

Tissue Preparation

Aplysia californica were obtained from Charles Hollahan (Santa Barbara, CA), kept in an aquarium until use, and anesthetized with an injection of isotonic $MgCl_2$ solution equal to 50% of the animal's body weight.[15, 28] The abdominal ganglion, with the attached pleural-abdominal connectives and the pleural-pedal ganglia, were isolated and stored in artificial sea water (ASW) containing (in mM): 460 NaCl, 10 KCl, 10 $CaCl_2$, 22 $MgCl_2$, 6 $MgSO_4$, and 10 N-2-hydroxyethylpiperazine-N'-2-ethanesulfonic acid (HEPES) (pH 7.8).[15]

Before sectioning, a solid block of agarose gel was created by pouring a heated saturated solution of agarose IV (Sigma-Aldrich, St. Louis, MO) into a Petri dish where it solidified. The agarose block was freeze-mounted with a few drops of water added onto an HM 550 microtome (Microm International, Walldorf, Germany) sample stage, and a smooth surface aligned to the cutting plane was created with the microtome by sectioning through the top layers of agarose. The abdominal ganglion was oriented on top of the newly created surface by holding and moving the pleural-abdominal connectives with forceps. A small amount of deionized water was added to the sample to improve freeze-mounting. Tissue sections of 10 μm thickness were cut at −20 °C using the microtome. A Parafilm M bead substrate at room temperature was placed above the tissue slice positioned on the metal microtome section stage surface and manual pressure was applied using the wooden handle end of an artist's brush. The relative orientation of the sample on the bead substrate, in comparison to the orientation of the ganglia on the cutting stage, and the perimeter of the sample edges are marked with a marker on the back side of the Parafilm M layer. To allow maximal analyte extraction while the sample is still partially wet and to reduce bead clumping, the samples were immediately manually stretched and placed onto conductive indium tin-oxide (ITO)-coated glass slides. The excess Parafilm M was manually torn off the glass slide edges, followed immediately by coating with

MALDI matrix. In addition, adjacent intact serial tissue slices were placed on a glass slide and optical images were taken.

MALDI Matrix Application, Condensation, and Metal Coating

Samples were coated with 30 mg/mL of 2,5-dihydroxybenzoic acid (DHB) (Sigma-Aldrich) matrix solution in 50:50 acetone:water. Coating was done with an artist's spray brush (Thayer & Chandler, Kenosha, WI) at a distance of ~30 cm in eight brief (~1 s) passes followed by drying for 1–2 min. The extent of drying and matrix accumulation was visually monitored during drying periods using light microscopy. Total matrix application time was about 15 min per sample. The samples were then rehydrated using a laboratory constructed humidity-controlled chamber equipped for automated thermal cycling of the sample adapted from our previously reported protocol.15 The new system consisted of a Peltier device (Ferrotec, Bedford, NH), a temperature controller with a panel interface (Ferrotec Bedford, NH), a thermistor (Ferrotec, Bedford, NH), a water-cooled heat sink (D-Tek Customs, Mission Viejo, CA), and a DC power supply. The Peltier device was controlled with a temperature cycle program via the FTC1000 software package (Ferrotec, Bedford, NH). The relative humidity of the chamber was adjusted to 85–95% with the sample placed on top of the Peltier device. The thermal cycling program was then initiated: the sample was cooled over 60 s to 14 °C and then held at 14 °C for 90 s, then warmed over 60 s to 28 °C and then held at 28 °C for 150 s. This cycling was repeated 3 times (~18 min) and then the temperature was held at 28 °C until the sample was completely dry. Throughout this process the sample could be visualized in real time using a CCD camera (DFW-X700, Sony, Tokyo, Japan) attached to a 7× zoom microscope (Edmund Optics, Barrington, NJ) to ensure that water pooling did not occur. After condensation, to increase signal obtained from the tissue and to reduce surface charging during imaging, the stretched sample surface was sputter-coated with a mixture of gold and paladium29, 30 for 15 s with a DESK II TSC turbo sputter coater (Denton, Moorestown, NJ).

Geometry File Creation for Automated Data Acquisition

In contrast to the previous method,[22] which used a 1 mm calibration bar to calibrate pixel spacing, the new method described here uses laser-melted holes in the membrane to create a spatial calibration grid. The MALDI laser repetition rate was increased to 200 Hz at maximal laser power to melt beam-sized holes in the membrane at a regular array of positions, as specified in the MTP Slide Adapter II geometry file, included in the Bruker FlexControl 3.0 software (Bruker Daltonics, Billerica, MA). Subsequent to matrix application and melting of holes in the membrane, optical images were taken of the stretched sample and the bead positions were located via light thresholding using ImageJ and the Colour Threshold plugin, as described previously.[22]

With a new in-house written Java code (available at http://www.neuroproteomics.scs.uiuc.edu/imaging.html), the pixel coordinates of the beads in the stretched sample image are converted directly into the fractional distance coordinates that are used in the Bruker geometry file format. The distance between each melted hole in the regular array is 0.0870 fractional distance units, as determined from the Bruker MTP Slide Adapter II geometry file, and the scaling is determined by dividing this value by the average distance in pixels, as measured in ImageJ, between the melted holes of the array in the stretched sample image (Eq. 1). The scaling is multiplied by the X and Y pixel coordinates corresponding to each bead to give the bead location in fractional distance coordinates (Eq. 2).

$$\frac{0.0870_{frac.dist.}}{\langle \text{array\_spacing} \rangle_{\text{pixels}}} = \text{scaling}_{\frac{frac.dist.}{\text{pixels}}} \quad (1)$$

$$\text{scaling}_{\frac{frac.dist.}{\text{pixels}}} \times XY\text{coordinate}_{\text{pixels}} = XY\text{coordinate}_{frac.dist.} \quad (2)$$

Besides scaling, the origin must be matched between the two coordinate systems by taking screen images in FlexControl of the melted holes and matching these visually with the holes in the stretched sample image to determine their pixel coordinates. It should be noted that the spatial accuracy of the geometry file alignment with bead positions decreases with the distance from the origin of the geometry file; this is due to the imprecision of coordinate system scaling. Therefore, multiple origins, called anchor points, are used to create four coordinate origins spaced throughout the sample. Bead positions in the geometry file are then calculated from their nearest anchor point.

Automated data acquisition is done at the locations of the individual bead positions using the sample-tailored geometry files with the AutoXecute function of FlexControl on an Ultraflex II TOF-TOF mass spectrometer (Bruker Daltonics) equipped with a solid-state UV laser and operated in positive ion mode. The laser repetition rate was set at 50 Hz with 100 repetitions at each bead location. Mass calibration was done in FlexControl with the aid of diluted Peptide Calibration Standard II (Bruker Daltonics) spotted onto the Parafilm M surface and mixed with MALDI matrix before the start of the imaging run. The total acquisition time for imaging the stretched abdominal ganglion sample containing 1839 beads was 2.3 h, and 5.4 h for the pleural-pedal ganglia sample of 4277 beads. The area of the imaged beads that contains tissue is smaller than the area of the total number of beads used in each experiment.

Image Reconstruction

Before image reconstruction, the data is processed and converted into a text file format, which is read by the in-house written Java code used to produce reconstructed ion images. Raw Bruker fid spectrum files from the imaging run were converted into text files as previously reported.[22] The in house-written MATLAB, version 7.2, R2006a (The MathWorks, Natick, MA), wrapper code for batch conversion of mzXML files into text files was modified to include baseline subtraction of each spectrum with the msbackadj.m function[31] from the Bioinformatics Toolbox 3.0, and to smooth each spectrum with the mslowess.m function, using the default processing parameters. The msbackadj.m function estimates the baseline through a moving window of 200 data points in width followed by regressing the baseline to the estimates with a spline approximation. The mslowess.m function smoothes spectra through a locally weighted linear regression with a linear polynomial fitting with a moving window of 10 data points in size.

Image reconstruction using a free transform process and plotting of ion images is done as described previously[22] with the aid of an in-house written Java code (www.neuroproteomics.scs.uiuc.edu/imaging.html). Resulting ion images present two-dimensional plots of the distribution and intensity of the analytes of interest, determined by taking the maximum signal intensity value selected from each analyzed mass spectrum within

a 2 Da window surrounding the targeted *m/z* value. For the resulting reconstructed abdominal ganglion images, a rotation of five degrees is necessary so that the signals originating from the left upper quadrant, specifically the LUQIN peptide (*m/z* 1200), used here as a marker peptide, are aligned with the expected biological location. This ensures that the ion image is co-registered with the orientation of the optical image of the adjacent serial tissue slice.

RESULTS AND DISCUSSION

To enable tissue section imaging, several improvements to the stretched imaging approach are described, including modified matrix application, methods for tracking tissue orientation, and a more accurate geometry file creation process. Sampling optimization includes the use of solid agarose surfaces aligned to the sectioning plane for tissue positioning and sectioning, and metal coating of samples to reduce surface charging. Lastly, a method for spectra batch processing facilitates peak picking in low quality spectra. These improved MSI protocols are then validated by comparing MS images of neuropeptide distributions in the *Aplysia* nervous system with previously published neuropeptide distribution maps.

The first step is to form the bead monolayer on the stretchable membrane substrate, which is placed between the surface of two glass slides to spread the beads over the membrane. To more effectively create a hexagonally packed bead monolayer on the Parafilm M layer, slight manual pressure is created against the membrane using an index finger moving in a circular motion. Too great a force results in formation of bi- or trilayers of beads and deformation of the Parafilm M sheet. Excess beads on top of the bead monolayer are removed with a stream of nitrogen gas, followed by another application of more intense manual pressure to embed the beads, ensuring a stronger mechanical contact between beads and the Parafilm M.

Improved results are achieved if the tissue section is stretched immediately after it is loaded onto the bead array surface while the tissue is still wet. Immediate stretching of an elastic wet tissue sample enhances fragmentation[15] and reduces tissue/bead clumping that can occur in dried *Aplysia* ganglion sections (see Figure 1). Uniform tissue fragmentation, without bead clumping, is necessary for successful image reconstruction. In addition, immediate application of MALDI matrix after the tissue sectioning and fragmentation steps, while the tissue is partially wet, improves the quality of molecular ion signals. This may be due to increased analyte extraction efficiency from wet tissues. The shorter the timeframe between sample preparation and placing it on the membrane, stretching, and matrix application, the greater the likelihood of generating high quality images. Therefore, we take the required optical image of the bead-loaded, pre-stretched membrane before the tissue is applied to the bead surface, rather than after.

Continuous tracking of tissue orientation inside the microtome cryochamber while sectioning, during transfer to the bead substrate, and during stretching, maintains the tissue alignment. This alignment allows comparison of the resulting ion images with the morphological features in the optical images of adjacent tissue sections. Previously,[15] we embedded the sample onto a piece of *Aplysia* buccal muscle for more repeatable sectioning of unfixed tissues. Unfortunately, this approach was slow and limited our ability to perform quick positioning and orienting of the tissue in the desired sectioning plane. We now create an agarose surface aligned with the plane and place tissues on top of this surface. Pressing the bead substrate onto the tissue slice located on the cold microtome sample stage, instead of the original approach of transferring the tissue to the bead substrate with an artist's brush,[17] allows the sample orientation to be tracked and marked on the membrane. A room temperature bead substrate that is warmer than the tissue facilitates complete transfer of the sample onto the bead array. Labeling of the sample orientation and its perimeter with a marker on the back of the membrane is followed immediately by sample stretching. The perimeter markings aid in placing the

appropriate section of the stretched Parafilm M membrane containing the sample onto the glass slide after stretching.

During matrix application, the use of a light microscope to observe both the quality of MALDI matrix crystal coverage and the drying process in between successive spray coatings effectively guides the matrix application process. A further increase in relative intensity of analyte signal can be achieved by assuring that the sample is conductive, thus eliminating buildup of electrical charge on the sample surface. This is done either by placing the stretched sample onto ITO glass slides or coating the sample with a thin layer of metal.[29] Samples that used both treatments, the conductive ITO slide and metal coating, were found to result in only slightly better analyte signal than either approach alone, and so the ITO-coated slides alone were used here. Using both steps may still be helpful if the Parafilm M membrane has poor contact with the conductive ITO slide surface.

After melting the guide markers in the Parafilm M surface and MALDI matrix application, and before creation of geometry files, a transmission mode optical image is taken of the stretched sample. Taking the bead image in grazing angle incident light helps to illuminate the bead positions for more effective light thresholding in ImageJ. However, bright light also makes the melted Parafilm M markers that serve as anchor points less visible. A separate image of the sample at lower exposure levels was often used to aid in visualizing the holes (Figure 1A).

This new geometry file creation method improves the spatial accuracy of determining the individual bead locations. In our previous method,[22] the value of the pixel scaling had a precision of several pixels over several millimeters, but had greater errors over longer distances so that the accuracy of indicating bead positions decreased for larger samples. Here the conversion is calculated by directly converting pixel coordinates into fractional distance coordinates using the laser-melted holes in the stretched sample image as the spatial calibration points. The value of the scaling is more accurately determined, making the geometry file more accurate over larger areas. Besides determination of scaling, the melted markers are also used as anchor points between the stretched sample optical image and the Ultraflex II coordinate system. Even with larger area samples such as in the ~4000 bead pleural-pedal sample described below, use of several melted anchor points allow the creation of an accurate geometry file covering the entire sample; here each bead position in fractional distance coordinates is calculated using the corresponding nearest melted anchor point as the origin.

Data processing is used to improve the quality of the reconstructed molecular ion images. The quality of analyte signal from each spot depends on many parameters, including the presence of signal suppression from highly abundant species, the degree of co-crystallization of analyte and MALDI matrix, and the presence of high concentrations of inorganic salts. It is not surprising that the peptide signals acquired from tissue fragments located on some beads have lower intensities and appear in spectra with a range of background chemical and/or digitization noise. Therefore, the *mslowess* function in MATLAB is a function that provides local weighted scatter plot smoothing,[32] a linear local regression smoothing operation with a moving window that effectively reduces noise. The resulting smoothed signals allow more accurate peak picking by an in-house written Java code. Also, baseline subtraction over separate windows of 200 data points with the *msbackadj* function[31] helps to reduce any influence of varying mass spectra quality on the quality of the final molecular ion image. Background subtraction is important in MSI experiments, otherwise a varying background may add noise or even false-positive analyte detection to ion distribution images. These processing steps can allow peptides to be detected from spectra that would have appeared to only contain noise.

The spectral quality has been compared between traditional imaging experiments using an automated matrix application via the ImagePrep (Bruker Daltonics)[33, 34] and stretched

imaging experiments, demonstrating that the recondensation/recrystallization procedure that desalted intact tissue samples23 also works for stretched tissue samples (Figure S-1 in the Supporting Information).

How well do these protocols work for the determination of peptide localization within tissue sections using MALDI-MSI? Because most peptides have yet to be MS imaged at cellular resolution, we use the *Aplysia* CNS to validate our approach. The abdominal ganglion, located in the animal's visceral body cavity, innervates the peripheral organs of the animal. This ganglion is a part of the CNS that also contains a group of the head ganglia. The branchial nerve extending from the abdominal ganglion can be seen in the lower right portion of the optical image of a serial tissue section in Figure 2A and can be used as a morphological reference point. Of the three different *Aplysia* ganglia imaged here, the abdominal ganglion has been the most thoroughly investigated by physiological,[35] molecular biological,[36] and chemical techniques.[37-39] The peptide content of numerous abdominal ganglion cells and cell populations has been reported, including prohormone expression and its post-translational processing.

Validation of the ion images produced by the stretched imaging method can therefore be performed via comparison to previously reported *in situ* and immunostaining results. For example, neuropeptide Y (NPY) is known to stimulate and regulate food intake in *Aplysia*, and has homologous peptides in vertebrates that are associated with stress.[40, 41] MALDI profiling has previously shown localization of NPY to the lower right quadrant on the ventral side of the abdominal ganglion and possibly to the RG cluster.[42] The distribution of ions match the *m/z* ratios of NPY in Figure 2B and C-flanking peptide of neuropeptide Y (CPON) in Figure 2C, indicating that both peptides are colocalized to the bottom-central region of the tissue slice, likely occupied by a portion of the RG cluster where NPY and related peptides were previously reported.[42] In addition, one of the R3-14 prohormone-related peptides that mediates cardiac output[43] is detected in the upper portion of the ganglion (Figure 2D). Signals corresponding by molecular mass to other R3-14 related peptides are detected in various other locations in the ganglion (data not shown). This is expected as R3-14 peptides are known to be transported throughout this ganglion.[44] Another example involves the R15 peptides that are encoded by an alternatively spliced R15 peptide gene,45 which are thought to have broad regulatory functions, including excitatory effects on heart muscle and coordination of autonomic neural regulation with escape locomotion.7, 46 R15 peptides are known to be located in the R15 giant neuron, in the heart exciter neuron RB_{HE}, and in the L9G gill motoneurons, as well as in the deeply located L40 cell, all of which have extensive projections throughout this ganglion.[7] Accordingly, a distribution of ions with *m/z* values corresponding to those of the R15-prohormone related peptides are shown in Figure 2E,F. These analytes are colocalized in the bottom and central regions of the ganglion slice image that correspond to the location of the R15-peptide expressing neurons. Egg-laying hormone (ELH) originates from bag cell clusters located at the rostrolateral part of the ganglion, Figure 2G.[47] ELH, when injected into an animal, is sufficient to cause egg laying. The distribution of ions in the slice ion image, mass matching an ELH-related peptide called delta bag cell peptide, is shown in Figure 2H. The signal, located at the top of the MS image near the area occupied by bag cell clusters, as well as in other regions of the image, may result from the presence of these peptides in bag cell neuron projections to the neuropil, a dense tangle of neuronal processes in the center of the ganglion.[48]

Figure 3 shows a different set of ion images from the abdominal ganglion; panels A–C show the MSI results that fit previous published maps of mRNA expression or immunoreactivity for several known *Aplysia* prohormones (or for prohormone-related peptides) that are shown in panels D–F. Pedal peptide is widely expressed throughout the *Aplysia* nervous system.49 In the immunostaining results shown in panel D, the dotted circles represent cells with high immunoreactivity for pedal peptide, matching the distribution of mass-matched ions from panel

A. However, the filled circles in panel D indicate several cells labeled via the prior immunostaining where we did not detect the peptide with MSI, perhaps caused by sectioning of the tissue at an angle that did not appreciably intersect these cell somata. LUQIN peptide, a peptide that triggers the closing of the renal pore, is located in the left upper quadrant cells, 50, [51] and the ion image of mass matched LUQIN peptide in panel B correlates to the immunostaining map in panel E. We recently reported the existence and localization of the feeding circuit-activating peptides (FCAPs),[52] which initiate motor activity related to feeding behaviors. These peptide distributions, studied by *in situ* hybridization and immunohistochemistry, are shown to localize in the center of the ganglion on its dorsal side and in the bag cells,[52] as seen in panel F. Ions corresponding to one of the FCAPs were detected in areas of the tissue slice that correspond to the bag cells but not in the center of the slice (Panel C). This may be a result of sectioning the ganglion at a layer that did not intersect with those specific positive cells, or perhaps the concentration of the analytes was below their limits of detection in those cells.

While the abdominal ganglion provided validation of the stretched imaging method to detect and properly reconstruct ion images, the pleural-pedal ganglia, which are not as well-characterized, offer the opportunity to gain new information on the localization of known and putative peptides using the ion distribution maps obtained with our optimized stretched sample imaging protocol.

Figure 4A shows an optical image of a serial section of the left pleural-pedal ganglia sectioned near the dorsal surface. Figure 4B,C shows the distribution of ions *m/z* 1545 and *m/z* 1680 that correspond to calculated molecular ion masses of monoprotonated peptides from the recently reported novel *Aplysia* prohormone pleurin (GenBank accession number AY833131). These images show two possible amidated peptide products from the pleurin prohormone that closely colocalize, although the distribution of the analyte with *m/z* 1545 extends slightly more into the pedal ganglion, panel B. The ion images in panels D–F show putative ions at *m/z* 1990 and *m/z* 1970 in panels D and E that colocalize in the pleural ganglion and in the center of the pedal ganglion, and an unknown at *m/z* 1599 in panel F that is localized only to the pedal ganglion. Ion images are also shown of mass matched peptide distributions that closely align with previously reported immunoreactivity maps of known peptides from the pleural pedal ganglia (Figure S-2 in the Supporting Information).

CONCLUSIONS

A set of improved protocols for the stretched sample method have been demonstrated that enable the imaging of neuropeptides in tissue sections. The analyte distribution images from ganglia of *Aplysia californica* are similar to those produced using other approaches. The stretched imaging approach offers several advantages compared to traditional MS imaging, such as the reduction of inorganic ion adducts and analyte redistribution during sample preparation, and the ability to detect and spatially localize low abundant or sparse analytes. The optimized protocols are easily implemented for imaging tissue sections. Tissue stretching and profiling has been demonstrated on mammalian spine and other tissues[8, 53] and so the imaging protocols are suitable for a variety of tissue types besides the *Aplysia* ganglia used here. Stretched imaging has applications in MS imaging of morphologically and chemically heterogeneous structures in the nervous system where changes in neuropeptide expression and transport caused by activity dependent changes, drugs of abuse or progressive disease states[54] can be spatially localized. Another exciting application complements peptidomics studies from newly characterized animal models after a number of new prohormones are discovered; [55-57] the stretched sample imaging method can be used in a global fashion to determine peptide distributions without the need to develop specific antibodies for literally dozens of new prohormones and hundreds of new neuropeptides.

Supplementary Material

Refer to Web version on PubMed Central for supplementary material.

Acknowledgments

The authors would like to thank Scott J. Robinson and Eric B. Monroe for valuable discussions and assistance. The project described was supported by Award No. DE018866 from the National Institute of Dental and Craniofacial Research (NIDCR) and the Office of the Director, National Institutes of Health (NIH), and the National Institute on Drug Abuse under Award Nos. DA017940 and P30DA018310. The content is solely the responsibility of the authors and does not necessarily represent the official views of the NIDCR, NIDA or NIH.

REFERENCES

(1). DeKeyser SS, Kutz-Naber KK, Schmidt JJ, Barrett-Wilt GA, Li L. J. Proteome Res 2007:1782–1791. [PubMed: 17381149]

(2). Li L, Sweedler JV. Annu. Rev. Anal. Chem 2008;1:451–483.

(3). Wisztorski M, Croix D, Macagno E, Fournier I, Salzet M. Dev. Neurobiol 2008;68:845–858. [PubMed: 18383549]

(4). Trim PJ, Atkinson SJ, Princivalle AP, Marshall PS, West A, Clench MR. Rapid Commun. Mass Spectrom 2008;22:1503–1509. [PubMed: 18421763]

(5). Rubakhin SS, Churchill JD, Greenough WT, Sweedler JV. Anal. Chem 2006;78:7267–7272. [PubMed: 17037931]

(6). Caprioli RM, Farmer TB, Gile J. Anal. Chem 1997;69:4751–4760. [PubMed: 9406525]

(7). Romanova EV, McKay N, Weiss KR, Sweedler JV, Koester J. J. Neurophysiol 2007;97:481–491. [PubMed: 17228083]

(8). Monroe EB, Annangudi SP, Hatcher NG, Gutstein HB, Rubakhin SS, Sweedler JV. Proteomics 2008;8:3746–3754. [PubMed: 18712768]

(9). Deininger S-O, Ebert Matthias P. Fütterer Arne, Gerhard Marc, Röcken C. J. Proteome Res 2008;7:5230–5236. [PubMed: 19367705]

(10). Chen R, Hui L, Sturm RM, Li L. J. Am. Soc. Mass Spectrom 2009;20:1068–1077. [PubMed: 19264504]

(11). Bailey CH, Chen M. Science 1983;220:91–93. [PubMed: 6828885]

(12). Gingrich KJ, Byrne JH. J. Neurophysiol 1985;53:652–669. [PubMed: 2580065]

(13). Kruse R, Sweedler JV. J. Am. Soc. Mass Spectrom 2003;14:752–759. [PubMed: 12837597]

(14). Hummon AB, Amare A, Sweedler JV. Mass Spectrom. Rev 2006;25:77–98. [PubMed: 15937922]

(15). Monroe EB, Jurchen JC, Koszczuk BA, Losh JL, Rubakhin SS, Sweedler JV. Anal. Chem 2006;78:6826–6832. [PubMed: 17007502]

(16). Li L, Romanova EV, Rubakhin SS, Alexeeva V, Weiss KR, Vilim FS, Sweedler JV. Anal. Chem 2000;72:3867–3874. [PubMed: 10959975]

(17). Zimmerman, TA.; Monroe, EB.; Tucker, KR.; Rubakhin, SS.; Sweedler, JV. Biophysical Tools for Biologists, Volume Two: In Vivo Techniques. Correia, JJ.; Detrich, HW., editors. Vol. Vol. 89. Elsevier; San Diego: 2008. p. 361-390.

(18). Altelaar AFM, Taban IM, McDonnell LA, Verhaert PDEM, Lange R. P. J. d. Adanc RAH, Mooid WJ, Heeren RMA, Piersma SR. Int. J. Mass Spectrom 2007;260:203–211.

(19). Baluya DL, Garrett TJ, Yost RA. Anal. Chem 2007;79:6862–6867. [PubMed: 17658766]

(20). Chen Y, Allegood J, Liu Y, Wang E, Cachón-González B, Cox TM, Merrill AH, Sullards MC. Anal. Chem 2008;80:2780–2788. [PubMed: 18314967]

(21). Aerni H-R, Cornett DS, Caprioli RM. Anal. Chem 2006;78:827–834. [PubMed: 16448057]

(22). Zimmerman TA, Monroe EB, Sweedler JV. Proteomics 2008;8:3809–3815. [PubMed: 18712762]

(23). Monroe EB, Koszczuk BA, Losh JL, Jurchen JC, Sweedler JV. Int. J. Mass Spectrom 2007;260:237–242.

(24). Ma M, Wang J, Chen R, Li L. J. Proteome Res 2009;8:2426–2437. [PubMed: 19222238]

(25). Wang J, Chen R, Ma M, Li L. Anal. Chem 2008;80:491–500. [PubMed: 18189446]
(26). Marinesco S, Duran KL, Wright WG. J. Physiol 2003;550:241–253. [PubMed: 12740422]
(27). Stuart DK, Strumwasser F. J. Neurophysiol 1980;43:499–519. [PubMed: 6892928]
(28). Giardino ND, Aloyz RS, Zollinger M, Miller MW, Desgroseillers L. J. Comp. Neurol 1996;374:230–245. [PubMed: 8906496]
(29). Altelaar AFM, Klinkert I, Jalink K, Lange R. P. J. d. Adan RAH, Heeren RMA, Piersma SR. Anal. Chem 2006;78:734–742. [PubMed: 16448046]
(30). McCombie G, Staab D, Stoeckli M, Knochenmuss R. Anal. Chem 2005;77:6118–6124. [PubMed: 16194068]
(31). McDonald RA, Skipp P, Bennell J, Potts C, Thomas L, O'Connor CD. Expert Syst. Appl 2009;36:5333–5340.
(32). Cho H, Smalley DM, Theodorescu D, Ley K, Lee JK. Proteomics 2007;7:3681–3692. [PubMed: 17879999]
(33). Gustafsson JOR, McColl SR, Hoffmann P. J. Proteomics Bioinf 2008;1:458–463.
(34). McDonnell LA, van Remoortere A, van Zeijl RJ, Deelder AM. J. Proteome Res 2008;7:3619–3627. [PubMed: 18570456]
(35). Hatcher NG, Sweedler JV. J. Neurophysiol 2008;99:333–343. [PubMed: 18003877]
(36). Song Y, Liu Y-M. J. Mass Spectrom 2008;43:1285–1290. [PubMed: 18416437]
(37). Ewing MA, Wang J, Sheeley SA, Sweedler JV. Anal. Chem 2008;80:2874–2880. [PubMed: 18341354]
(38). Jung LJ, Scheller RH. Science 1991;251:1330–1335. [PubMed: 2003219]
(39). Li L, Garden RW, Sweedler JV. Trends Biotechnol 2000;18:151–160. [PubMed: 10740261]
(40). Jing J, Vilim FS, Horn CC, Alexeeva V, Hatcher NG, Sasaki K, Yashina I, Zhurov Y, Kupfermann I, Sweedler JV, Weiss KR. J. Neurosci 2007;27:3490–3502. [PubMed: 17392465]
(41). Husum H, Mathé AA. Neuropsychopharmacol 2002;27:756–764.
(42). Garden RW, Shippy SA, Li L, Moroz TP, Sweedler JV. Proc. Natl. Acad. Sci. U.S.A 1998;95:3972–3977. [PubMed: 9520477]
(43). Newcomb R, Scheller RH. J. Neurosci 1987;7:854–863. [PubMed: 3549995]
(44). Kreiner T, Sossin W, Scheller RH. J. Cell Biol 1986;102:769–782. [PubMed: 3949877]
(45). Alevizos A, Karagogeos D, Weiss KR, Buck L, Koester J. J. Neurobiol 1991;22:405–417. [PubMed: 1890422]
(46). Skelton ME, Koester J. J. Comp. Physiol. A 1992;171:141–155. [PubMed: 1359129]
(47). Branton WD, Arch S, Smock T, Mayeri E. Proc. Natl. Acad. Sci. U.S.A 1978;75:5732–5736. [PubMed: 281720]
(48). Conn PJ, Kaczmarek LK. Neurosci 1989;27:363–371.
(49). Pearson WL, Lloyd PE. J. Neurosci 1989;9:318–325. [PubMed: 2913210]
(50). Koester J, Koch UT. Experientia 1987;43:972–980. [PubMed: 2888684]
(51). Koester J, Alevizosi A. J. Neurosci 1989;9:4078–4088. [PubMed: 2585067]
(52). Sweedler JV, Li L, Rubakhin SS, Alexeeva V, Dembrow NC, Dowling O, Jing J, Weiss KR, Vilim FS. J. Neurosci 2002;22:7797–7808. [PubMed: 12196603]
(53). Zimmerman TA, Rubakhin SS, Sweedler JV. Meth. Mol. Biol. 2010 (in press).
(54). Romanova EV, Hatcher NG, Rubakhin SS, Sweedler JV. Neuropharmacology 2009;56(Suppl 1):196–204. [PubMed: 18722391]
(55). Hummon AB, Richmond TA, Verleyen P, Baggerman G, Huybrechts J, Ewing MA, Vierstraete E, Rodriguez-Zas SL, Schoofs L, Robinson GE, Sweedler JV. Science 2006;314:647–649. [PubMed: 17068263]
(56). Bovine Genome Sequencing and Analysis Consortium. Science 2009;324:522–528. [PubMed: 19390049]
(57). Amare A, Sweedler JV. Peptides 2007;28:1282–1290. [PubMed: 17537543]

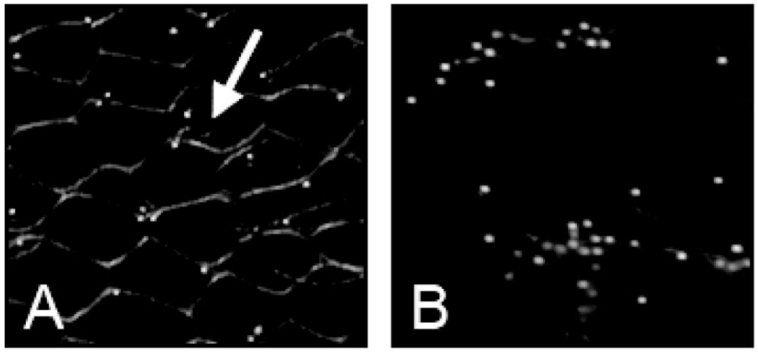

Figure 1.

The quality of dividing of tissue sections into relatively uniform small pieces depends on tissue properties. **(A)** Stretching the thin CNS section immediately after it is sectioned, while the tissue is still hydrated, results in improved tissue fragmentation. A marker hole formed in the Parafilm M membrane using the TOF mass spectrometer laser is labeled by the arrow. The marker holes match the beam profile of the laser and are used as spatial calibration and anchor points during the creation of sample-tailored geometry files for automated data acquisition. **(B)** If the sample stretching is done after the tissue dries, tissue/bead clumping is observed.

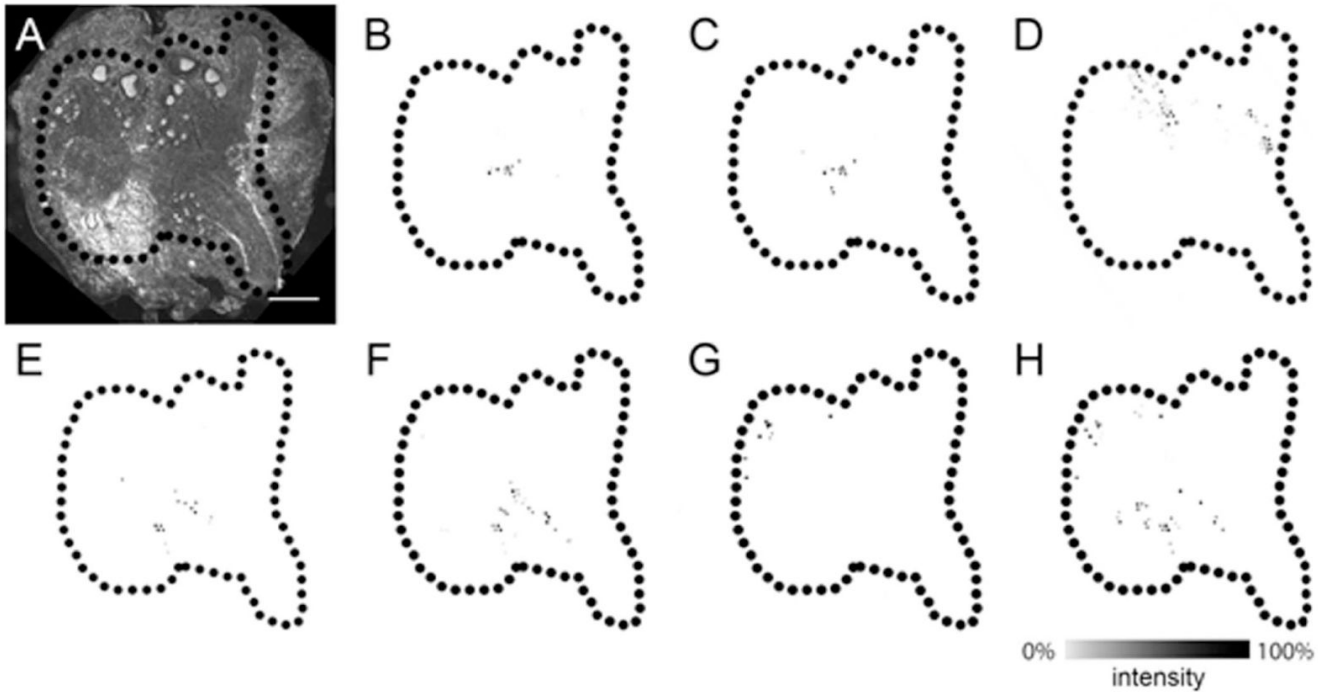

Figure 2.

Images of peptide distribution in the abdominal ganglion obtained after the image reconstruction procedure agree with previously published data on localization of the analytes obtained using a variety of approaches. **(A)** Optical image of a 10-μm thick abdominal ganglion section cut close to the dorsal surface. Scale bar = 1 mm. Reconstructed ion images of **(B)** neuropeptide Y at *m/z* 4688, **(C)** and C-flanking peptide of neuropeptide Y at *m/z* 2567, colocalize in the center of the sample near the RG cluster.[42] **(D)** R3-14 peptide at *m/z* 1381 is known to localize to the R cluster of giant neurons in the right upper quadrant of the dorsal side of the ganglion.[44] **(E,F)** Pyroglutaminated-R15-α peptide at *m/z* 3981 and R15-β peptide, *m/z* 2860, colocalize in the center of the ganglion, near the location of the R15 cell and RB_{HE} cells, where it is known to be expressed.[7] As expected, **(G)** egg-laying hormone is seen near the location of the bag cells at the top of the ganglion. **(H)** Delta bag cell peptide appears both near the location of the bag cells and in the middle areas of the ganglion.

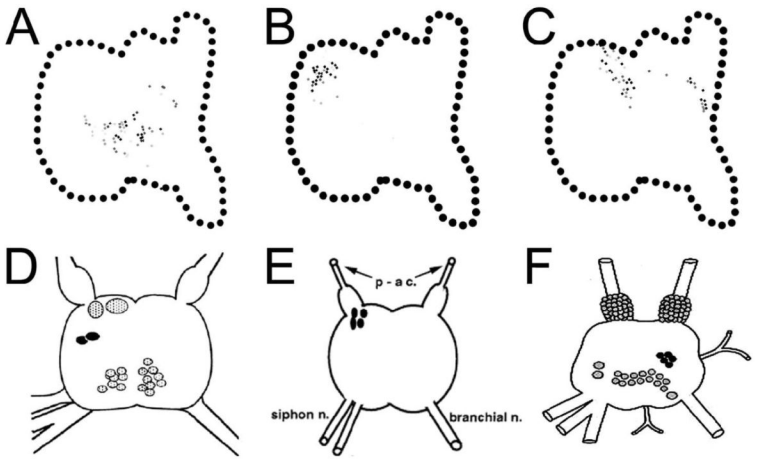

Figure 3.

(A–C) Peptide distributions observed from a 10-μm section of the abdominal ganglion prepared using the stretched sample approach are similar to **(D–F)** observations from immunohistochemical data from antibodies raised to the same prohormones. **(A)** Distribution of pedal peptide at *m/z* 1540 matches the distributions using immunostaining **(D)**,[49] as does **(B,E)** left-upper quadrant peptide at *m/z* 120028 and **(C,F)** feeding-circuit activating peptide, FCAP, at m/z 1369.[52] The FCAP-related peptide shown in panel C was detected in areas occupied mostly by the bag cells where presence of the FCAP prohormone has been shown previously by combined immunoreactivity and *in situ* hybridization. Panels D and F are adapted with permission from the Journal of Neuroscience from references [49] and [52], respectively. Panel E is adapted with permission from Wiley-Blackwell from reference [28].

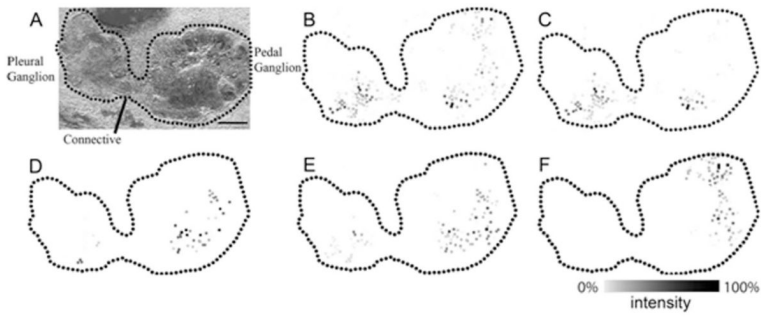

Figure 4.

(A) Optical image of a 10-μm section from close to the dorsal surface of the left pleural-pedal ganglia. Scale bar = 0.5 mm. **(B–F)** Reconstructed ion images of different peptide localizations in the tissue. **(B)** Pleurin peptide signals at *m/z* 1545 and **(C)** *m/z* 1680 colocalize in both ganglia. Localizations of putative novel neuropeptides at **(D)** *m/z* 1990, **(E)** *m/z* 1970, and **(F)** *m/z* 1599 do not match distributions of known peptides.